Hindawi
Journal of Nanomaterials
Volume 2020, Article ID 7915878, 13 pages
https://doi.org/10.1155/2020/7915878

Research Article

ZIF-67/*g*-C_3N_4-Modified Electrode for Simultaneous Voltammetric Determination of Uric Acid and Acetaminophen with Cetyltrimethylammonium Bromide as Discriminating Agent

Huynh Truong Ngo,[1,2] Le Thi Hoa,[1] Nguyen Tan Khanh,[3] Tran Thi Bich Hoa,[1] Tran Thanh Tam Toan,[1] Tran Xuan Mau,[1] Nguyen Hai Phong,[1] Ho Sy Thang,[4] and Dinh Quang Khieu[1]

[1]*University of Sciences, Hue University, 530000, Vietnam*
[2]*Department of Food Safety and Hygiene, Thua Thien Hue 530000, Vietnam*
[3]*University of Medicine and Pharmacy, Hue University, 530000, Vietnam*
[4]*Office of Graduate Affairs, Dong Thap University, 870000, Vietnam*

Correspondence should be addressed to Ho Sy Thang; hsthang@dthu.edu.vn and Dinh Quang Khieu; dqkhieu@hueuni.edu.vn

Received 4 September 2019; Revised 31 December 2019; Accepted 8 January 2020; Published 27 January 2020

Academic Editor: Alexander Pyatenko

In the present paper, the ZIF-67/*g*-C_3N_4 composite was synthesized and utilized as a modifier for a glassy carbon electrode for the simultaneous voltammetric determination of uric acid (URA) and acetaminophen (ACE) with cetyltrimethylammonium bromide (CTAB) as a discriminating agent. The composite was characterized using X-ray diffraction, scanning electron microscopy, transmission electron microscopy, X-ray photoelectron spectroscopy, and nitrogen adsorption/desorption isotherms. The obtained ZIF-67/*g*-C_3N_4 composite exhibits good textural properties (specific surface area: 75 $m^2 \cdot g^{-1}$) and is stable in water with a pH range of 3 to 10. The ZIF-67/*g*-C_3N_4-modified electrode combined with CTAB as a discriminating agent possesses excellent catalytic electrochemistry towards URA and ACE with well-defined electrochemical responses. The electrochemical kinetics study is also addressed. The linear relation of the oxidation peak current of URA and ACE and the concentration ranging from 0.2 μM to 6.5 μM provide a detection limit of 0.052 μM for URA and 0.053 μM for ACE. The proposed method is well-suited to simultaneously analyze URA and ACE in human urine with comparable results with HPLC.

1. Introduction

Uric acid (denoted as URA) is a heterocyclic compound with formula $C_5H_4N_4O_3$, which is the primary end product of purine metabolism. A high URA level in the blood can indicate the presence of numerous diseases and/or physiological disorders. A high concentration of URA in the urine and blood is observed in patients suffering from diseases such as gout and hyperuricaemia [1]. Acetaminophen (denoted as ACE) with formula $C_8H_9NO_2$, also known as paracetamol, is an effective pain killer used to relieve pains related to many parts of the body [2]. An ACE overdose can cause toxic metabolite accumulation, which may cause serious hepatotoxicity and nephrotoxicity [3].

Today, the speed, selectivity, sensibility, low detection limits, low cost, and *in situ* operation of electroanalytical techniques have been considered as the robust approaches to analyze organic or inorganic traces, especially in pharmaceutical compounds. Uric acid and ACE, as well as dopamine and ascorbic acid, exhibit the redox behaviour at similar potentials. The simultaneous detection of these compounds is sometimes difficult because of interfering overlapping effects. Employing separation steps such as chromatography can sometimes overcome this drawback, but it is usually an

expensive option. Therefore, the search for simple, inexpensive, sensitive, and accurate analytical approaches for the simultaneous detection of URA and ACE would be necessary. There exist two approaches to overcome these issues in electrochemical analysis: (i) using an electrode modified with hybrid nanomaterials to improve the interaction of electrospecies and electrode and subsequently increase the peak-peak separation of analytes and electrochemical signals. Phong et al. [4] studied the simultaneous determination of ascorbic acid, paracetamol, and caffeine using an electrochemically rGO-modified electrode. Kutluay and Aslanoglu [5] reported the selective determination of ACE in the presence of ascorbic acid, dopamine, and uric acid using a glassy carbon electrode modified with multiwalled carbon nanotubes. (ii) The second approach is to use the surfactants as a discriminating agent to promote the peak-peak separation. Surfactants are amphiphilic molecules that contain a hydrophilic group at the one end and a hydrophobic group at the other. Below the critical micelle concentration on the solid-liquid interface, the surfactants form a bilayer or hemimicelle structures [6, 7]. These special structures initiate the interface properties of the electrodes and consequently act as discriminating agents to enhance the resolution of electrodes when the voltammetric peaks of two oxidation or reduction species occur at similar potentials. Alarcón-Angeles et al. [8] reported using sodium dodecyl sulfate as a discriminating agent for the electrochemical determination of dopamine in the presence of ascorbic acid. Liu et al. [9] studied the selective determination of dopamine in the presence of ascorbic acid using cetyltrimethylammonium bromide (denoted as CTAB) as a masking agent.

Recently, graphitic carbon nitride (g-C_3N_4), which is a polymeric layered material, structurally analogous to graphene, has emerged as a prospective material for use in electrochemistry [10, 11]. Besides its thermal and chemical stability, graphitic carbon nitride possesses metal-free and multiple structural defects, tunable electronic structure, mechanical stability, and high electrical conductivity [12]. Zeolitic imidazolate frameworks (ZIFs) are a subclass of metal-organic frameworks (MOFs). ZIFs are topologically isomorphic with zeolites. They are formed from tetrahedral metal ions (e.g., Zn and Co) connected by imidazolate linkers [13]. ZIF-67 with isostructural SOD zeolitic topology is formed from cobalt ions and 2-methylimidazole. ZIF-67 has a porous structure, a large surface area, and a big amount of active sites, and therefore, it is applied to several fields such as as a catalyst, for separation, and for adsorption [14, 15]. However, ZIF-67 has poor stability and low electrical conductivity. This limits its application in electrochemistry. Combining the advantageous features of both ZIF-67 and g-C_3N_4, one can manufacture versatile materials for electrochemistry and other potential applications. Recently, Meng et al. [16] reported ZIF-67/g-C_3N_4 as an efficient photocatalyst for CO_2 reduction. To the best of our knowledge, little is known about the use of ZIF-67/g-C_3N_4 as an electrode modifier in the electrochemical analysis.

Responding to this gap of knowledge, this article presents the synthesis of the ZIF-67/g-C_3N_4 composite using the ultrasound/microwave-assisted approach. Then, the composite was employed as a modifier to develop a novel electrode for the simultaneous determination of URA and ACE with CTAB as a discriminating agent.

2. Experimental

2.1. Materials. Melamine ($C_3H_6N_6$, 99%), cobaltous nitrate hexahydrate ($Co(NO_3)\cdot 6H_2O$, 99%), 2-methylimidazole ($CH_3C_3H_2N_2H$, 99%), uric acid ($C_5H_4N_4O_3$, >99%), acetaminophen ($CH_3CONHC_6H_4OH$, >99%), and cetyltrimethylammonium bromide (denoted as CTAB, $CH_3(CH_2)_{15}N(Br)(CH_3)_3$, >98%), sodium hydroxide (NaOH, ≥97%), hydrochloric acid (HCl, 37%), glucose ($C_6H_{12}O_6$, ≥99%), sucrose ($C_{12}H_{22}O_{11}$, ≥99%), sodium oxalate ($Na_2C_2O_4$, ≥99%), sodium nitrate ($NaNO_3$, ≥99%), calcium chloride ($CaCl_2$, ≥98%), potassium sulfate (K_2SO_4, ≥98%), ammonium sulfate ($(NH_4)_2SO_4$, ≥99%), and potassium bicarbonate ($KHCO_3$, ≥99%) were obtained from Merck & Co., Germany. Phosphoric acid (H_3PO_4, 85%), acetic acid (CH_3COOH, ≥99.8%), and boric acid (H_3BO_3, 99%) were purchased from Daejung Co., Korea. A Britton-Robinson buffer (denoted as BR-BS) is used for the pH range from 2 to 10. It was prepared by mixing equal volumes of 0.04 M H_3BO_3 (2.04 g/100 mL), 0.04 M H_3PO_4 (2.8 mL of 85% H_3PO_4/100 mL), and 0.04 M CH_3COOH (2.3 mL of glacial CH_3COOH/100 mL) that has been adjusted to the desired pH with 0.2 M NaOH or 0.2 M HCl. The stock solution of 1×10^{-2} M URA and 1×10^{-2} M ACE was prepared daily. Standard solutions were prepared by diluting the stock solution with the BR-BS.

2.2. Apparatus. X-ray diffraction (XRD) analysis was performed on a D8 Advance Bruker anode X-ray diffractometer with Cu Kα ($\lambda = 1.5406$ Å) radiation. Nitrogen adsorption/-desorption isotherms were performed using a Micromeritics 2020 volumetric adsorption analyzer system. Samples were degassed by heating under vacuum at 180°C for 3 hours. The specific surface area of the samples was calculated using the Brunauer-Emmett-Teller (BET) model. X-ray photoelectron spectroscopy (XPS) was recorded on a Shimadzu Kratos AXIS ULTRA DLD spectrometer equipped with a Theta Probe ARXPS System (Thermo Fisher Scientific, UK). The peak fitting was performed by CasaXPS software. The transmission electron microscopy (TEM) and scanning electron microscopy (SEM) images were collected using a JEOL JEM-2100F (USA) and an SEM JMS-5300LV (USA), respectively. Electrochemical measurements were performed using a CPA-HH5 Computerized Polarography Analyzer (Vietnam). Voltammetric measurements were performed using a glassy carbon electrode (GCE, 2.8 mm diameter) or a ZIF-67/g-C_3N_4-modified GCE (ZIF-67/C_3N_4-GCE) as a working electrode, an Ag/AgCl/3 M KCl as a reference electrode, and a platinum foil auxiliary electrode.

High-performance liquid chromatography (HPLC) was also used to determine the concentration of URA and ACE. The measurements were performed on a Shimadzu 2030 HPLC system with the following parameters: UV-vis detector ($\lambda = 275$ nm) and C18 (250×4 mm; 5 μm) chromatographic column; mobile phase: mixture of phosphate buffer

pH 2.3/acetonitrile (35/65 *v*/*v*); flow rate of 1.5 mL·min^{-1}; and injection volume: 5 mL.

2.3. ZIF-67/g-C_3N_4 Preparation. *g*-C_3N_4 was synthesized according to the reference [17]. Briefly, melamine (10 g) was placed into a crucible with a cover under ambient pressure. Then, it was heated to 550°C for 4 h in nitrogen, and a yellow *g*-C_3N_4 powder was obtained. $Co(NO_3)\cdot 6H_2O$ (2 mM) and 2-methylimidazole (2 mM) were completely dissolved in ethanol (15 mL) separately. 36 mg *g*-C_3N_4 was added into the cobaltous nitrate solution at ambient temperature and treated with ultrasound for 1 hour. Then, the 2-methylimidazole solution was added to the suspension of *g*-C_3N_4 and cobalt nitrate. Next, the mixture was placed into a microwave device and irradiated for 15 minutes, resulting in a light purple precipitate (ZIF-67/*g*-C_3N_4). Finally, the precipitate was washed with ethanol three times and dried at 80°C in air.

2.4. Preparation of Electrodes. A glassy carbon electrode (GCE) (2.8 mm diameter) was polished using 0.05 mm alumina slurry and rinsed thoroughly with distilled water. The electrode was then purified under ultrasonic agitation in ethanol for 5 min. 2 milligrams of ZIF-67/*g*-C_3N_4 was dispersed in 1 mL methanol under ultrasonic agitation for 60 min, resulting in a homogeneous purple suspension. 5 μL of ZIF-67/*g*-C_3N_4 suspension was dropped on the electrode surface. Then, the modified electrode was then dried at ambient temperature to obtain a ZIF-67/*g*-C_3N_4/GCE.

2.5. Electrochemical Measurements. The electrochemical measurements of URA and ACE were performed using cyclic voltammetry (CV) and differential pulse voltammetry (DPV). The DPVs were recorded in the potential range from −100 mV to 600 mV at ambient temperature with the pulse amplitude of 50 mV in all cases.

2.6. Real Sample Determination. Three samples of human urine were used to test the method. In detail, 1.0 mL of the urine sample was spiked with URA and ACE and mixed with 1.0 mL of BS buffer solution to produce a 2.0 mL test solution. 150 μM CTAB was added. The proposed DPV method was applied to the determination of URA and ACE in the spiked solution.

3. Results and Discussion

3.1. Characterization of Materials. The ZIF-67/*g*-C_3N_4 composite was synthesized through mixing *g*-C_3N_4 with the Co (II)/imidazole solution in ethanol under the ultrasonic and microwave irradiation. The resulting solids were investigated using XRD analysis (Figure 1(a)). All characteristic peaks of ZIF-67 (Figure 1(a)) are indexed according to the simulated XRD pattern of ZIF-67 from the database (CCDC671073). As for C_3N_4 (Figure 1(b)), two characteristic diffraction peaks of the tetragonal phase for *g*-C_3N_4 appear at $2\theta =$ 13.4° and 27.5° corresponding to the crystal plane of (100) and (002), respectively, and are indexed according to JCPDS 87-1526 [18]. In the XRD pattern of ZIF-67/*g*-C_3N_4 (Figure 1(c)), all the characteristic peaks of *g*-C_3N_4 and ZIF-67 are reduced significantly but still clearly observed. During ultrasonic treatment, *g*-C_3N_4 could split into the small clusters of *g*-C_3N_4, and thus, its crystal structure practically collapses. Therefore, the XRD diffractions of *g*-C_3N_4 are not observed in Figure 1(c). The textural properties of *g*-C_3N_4, ZIF-67, and the composite were characterized using nitrogen adsorption/desorption isotherms. As represented in Figure 1(d), all the samples illustrate a type IV isotherm with an H3 hysteresis loop according to IUPAC classification. S_{BET} of *g*-C_3N_4 is 5 $m^2\cdot g^{-1}$, while ZIF-67 exhibits a large S_{BET} of 1,330 $m^2\cdot g^{-1}$ due to its highly ordered and uniform structure. It is worth noting that the specific surface area of ZIF-67/*g*-C_3N_4 increases significantly ($S_{BET} = 75\ m^2\cdot g^{-1}$) compared with that of pure *g*-C_3N_4. The large specific surface area results in the efficient adsorption of analytes during the electrochemical process.

The morphologies of the resulting samples are investigated with SEM and TEM. The TEM image of *g*-C_3N_4 (Figure 2(a)) exhibits nanorods with 50 nm diameters, while the morphology of ZIF-67 consists of uniform polyhedrons of 134.2 ± 5.6 nm in size (counted for 140 particles) (Figure 2(b)). It is possible that the bonding of Co^{2+} to N in g-C_3N_4 is less strong than that in 2-methylimidazole. Therefore, Co^{2+} cations first coordinate with the nitrogen atoms from g-C_3N_4, and while 2-methylimidazole (MI) is added, it reacts with N to form ZIF-67 particles of around 10-20 nm which are highly dispersed on the *g*-C_3N_4 matrix as shown in Figure 3(c). The synthesis of ZIF-67 concurrently with *g*-C_3N_4 may suppress the growth of ZIF-67 crystals. Consequently, its size is rather small compared with that of ZIF-67 synthesized without *g*-C_3N_4.

To determine the chemical composition and the elemental state of ZIF-67/*g*-C_3N_4, its XPS was performed (Figure 4). As can be seen in Figure 4(a), the composite mainly consists of C, N, and Co with binding energy at around 285, 400, and 795 eV, respectively. In the N1s core level spectrum (Figure 4(b)), two peaks at 399.03 and 400.9 eV are assigned to the sp^2-bonded nitrogen and π excitation of *g*-C_3N_4, respectively [19, 20]. In the C1s core level spectrum (Figure 4(c)), the four deconvoluted peaks appear at 284.78, 285.36, 287.24, and 288.78 eV. These peaks can be assigned to C–C sp^2 (284.78 eV) and C–C sp^3 (287.24 eV) in imidazole [21, 22], sp^2-bonded carbon (288.78 eV) in aromatic rings of *g*-C_3N_4 (N–C=N), and the C–C coordination of the surface adventitious carbon (285.36 eV) [12]. For the Co2p core level spectrum (Figure 4(d)), the duplex of Co2p appears at 779.85 eV for $Co2p_{3/2}$ with a satellite peak at 783.94 eV and at 795.71 eV for $Co2p_{1/2}$ with a satellite peak at 801.14 eV. The main peak-satellite peak separation is narrow at about ~4 and ~5.4 eV for $Co2p_{3/2}$ and $Co2p_{1/2}$, respectively. The difference between the main peaks and the satellites is an important characteristic of the oxidation state of the cobalt ion. A narrow separation of about 4~6 eV (found in our study) is typical for Co (II), whereas a larger difference of about 9~10 eV is often found in Co (III) [23]. Therefore, the Co ions in ZIF-67/*g*-C_3N_4 are divalent.

The stability of the electrode modifier in different acidic media is critical for the application in the electrochemical analysis. In the present study, the ZIF-67/*g*-C_3N_4 composite

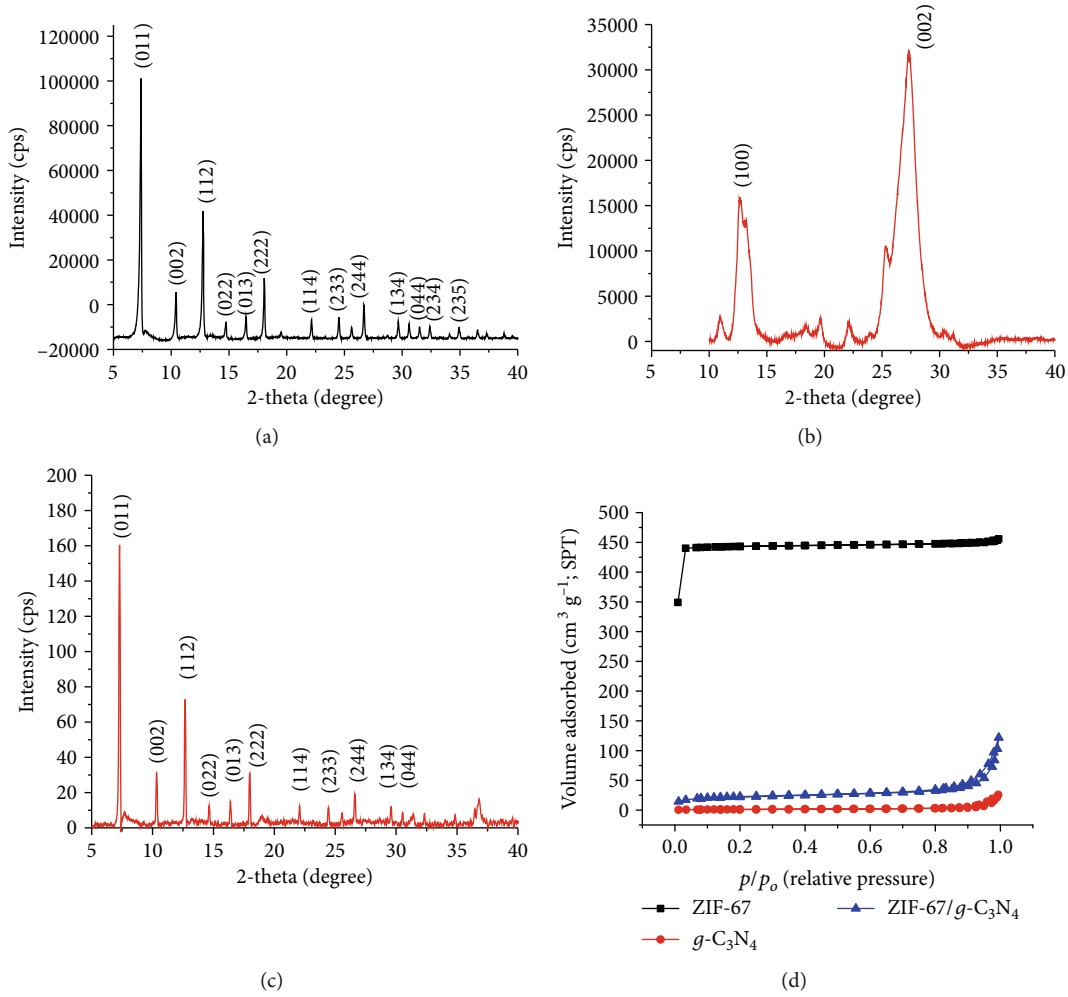

FIGURE 1: XRD patterns of (a) ZIF-67, (b) g-C_3N_4, and (c) ZIF-67/g-C_3N_4 and (d) nitrogen adsorption/desorption isotherms of ZIF-67, g-C_3N_4, and ZIF-67/g-C_3N_4.

was immersed in water with pH ranging from 1 to 11 for 10 hours (Figure 5). The stability of the composite was assessed via XRD measurement. At low pH (pH 1), the intensity of diffractions of this sample is reduced or even disappeared compared with the original ZIF-67/g-C_3N_4, and those of the samples at pH = 3 ÷ 12 seem slightly changeable, indicating that the composite is stable in aqueous solutions in this pH range.

3.2. Electrochemical Behaviour. Figure 6(a) represents the CVs at bare GCE, g-C_3N_4/GCE, ZIF-67/GCE, and ZIF-67-g-C_3N_4/GCE electrodes. As seen in the figure, the oxidation of URA and ACE occurs at similar potentials, and as a result, these two peaks are overlapped. However, the peaks are resolved significantly at the modified electrodes. The peak-to-peak separation is 0.10 V, 0.07 V, and 0.11 V for g-C_3N_4/GCE, ZIF-67/GCE, and ZIF-67/g-C_3N_4/GCE, respectively. The intensity of the oxidation peak for URA and ACE at ZIF-67/g-C_3N_4-GCE is 3.06 and 3.11 times as high as that at g-C_3N_4/GCE and 2.21 and 2.35 times as high as that at ZIF-67/GCE. These figures reveal that ZIF-67-g/C_3N_4 significantly promotes the electron transfer and, thus, oxidation of URA and ACE.

The peak current depends on the ZIF-67/g-C_3N_4 amount modified on the electrode surface (Figure 6(b)). ZIF-67/g-C_3N_4 enhances analyte adsorption. As a result, the peak current increases and reaches the maximum at the volume of the suspension of around 4 μL. Further increase of ZIF-67/g-C_3N_4 leads to a decrease in peak current because a thicker layer of adsorbed ZIF-67/g-C_3N_4 could reduce the electrical conductivity.

3.2.1. Effect of CTAB. The effects of CTAB concentration on the peak-to-peak separation of URA and ACE were performed by recording CVs of a series of solutions containing $C_{URA} = C_{ACE} = 0.5$ mM and various concentrations of CTAB (Figure 7(a)). As can be seen from Figure 7(b), the peak-to-peak separation (ΔE) increases with CTAB concentration and peaks at 150 μM CTAB ($\Delta E = 0.18$ V). Further increasing CTAB concentration leads to a slight reduction of ΔE. It is worth noting that the oxidation potential of ACE at 0.25 V seems to be constant, while the oxidation potential

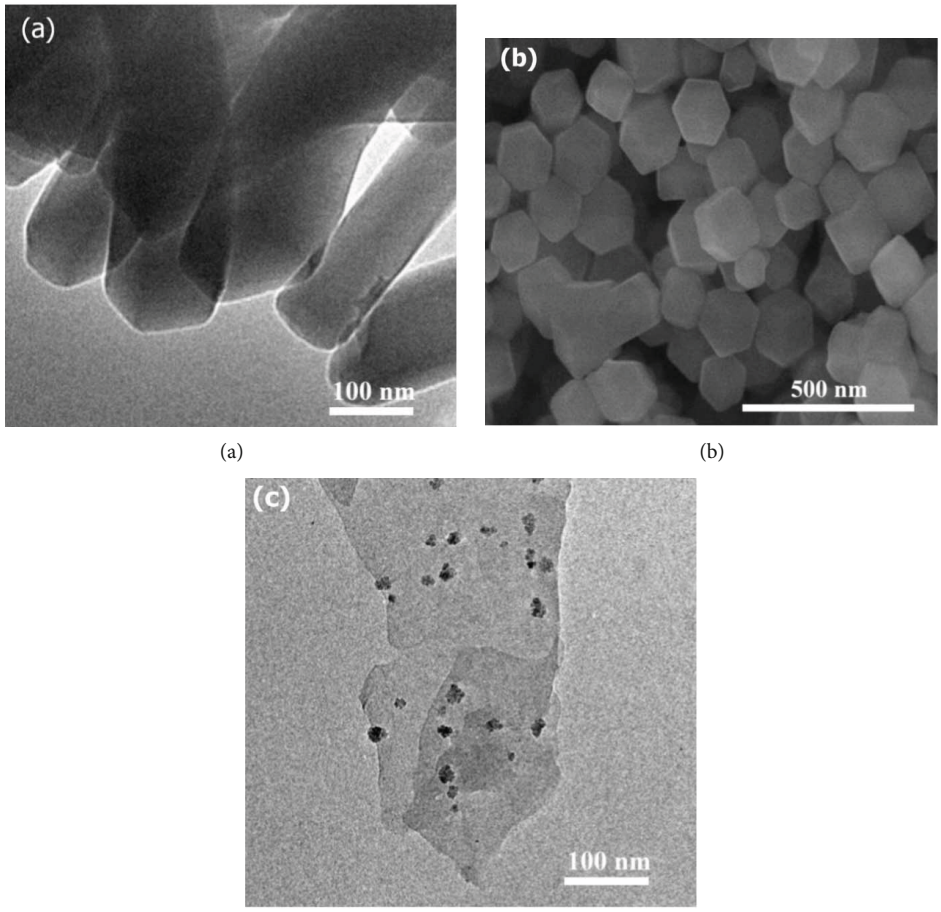

(a) (b)

(c)

Figure 2: (a) TEM of g-C_3N_4; (b) SEM of ZIF-67; (c) TEM of ZIF-67/g-C_3N_4.

of URA shifts to less positive values with increasing CTAB concentration. The possible reason would be that CTAB molecules aggregate on the surface of the modified electrode to form micelles for discriminating ACE from URA. The concentration of 150 μM for CTAB is suitable for further experiments.

3.2.2. Effect of pH. The CV curves at ZIF-67/g-C_3N_4-GCE were measured in the pH range from 7 to 10 (Figure 3(a)). The peak potential, E_p, reduces as pH increases, indicating that protons are involved in the redox processes (Figure 3(b)). The peak current, I_p, increases with pH and peaks at pH = 9. Further increase in pH causes a negligible change in the peak current (Figure 3(c)).

The anodic peak potential corresponds well to pH ranging from 7 to 10 with high correlation coefficients ($r = 0.985$ and 0.999) (Equations (1) and (2)):

$$E_{p,URA} = (0.34 \pm 0.03) + (-0.030 \pm 0.004) \times \text{pH}, \; r = 0.985, \tag{1}$$

$$E_{p,ACE} = (0.74 \pm 0.01) + (-0.056 \pm 0,001) \times \text{pH}, \; r = 0.999. \tag{2}$$

The slope of the oxidation peak potential of ACE vs. pH is 0.056 V/pH, which is very close to the theoretical value of 0.059 V/pH, corresponding to the equal number of protons and electrons in the redox process. The electrochemical oxidation of URA proceeding by a 2e/2 proton mechanism to yield a diimine is nowadays well established. Meanwhile, the value of 0.030 V/pH deviates significantly from the theoretical value of 0.0599 V/pH and is about its half, indicating that the electrode process is more complex in the studied pH and the number of transferred electrons may be twice as much as that of protons.

3.2.3. Effect of Scan Rate. Important information about the electrochemical mechanism can be derived from the relationship between the voltammetric signals (E_p and I_p) and the scan rate (denoted as ν). In the present study, the E_p and I_p dependence on the scan rate was investigated by using CVs (Figure 8(a)). If the electrooxidation reaction is reversible, E_p is independent on ν and vice versa. As can be seen from Figure 8(a), the peak potential increases with the scan rate. Therefore, the electron transfer in the URA and ACE electrooxidation is irreversible [24].

The linear plots of I_p vs. the square root of the scan rate ($\nu^{1/2}$) were established to assess whether the electrooxidation

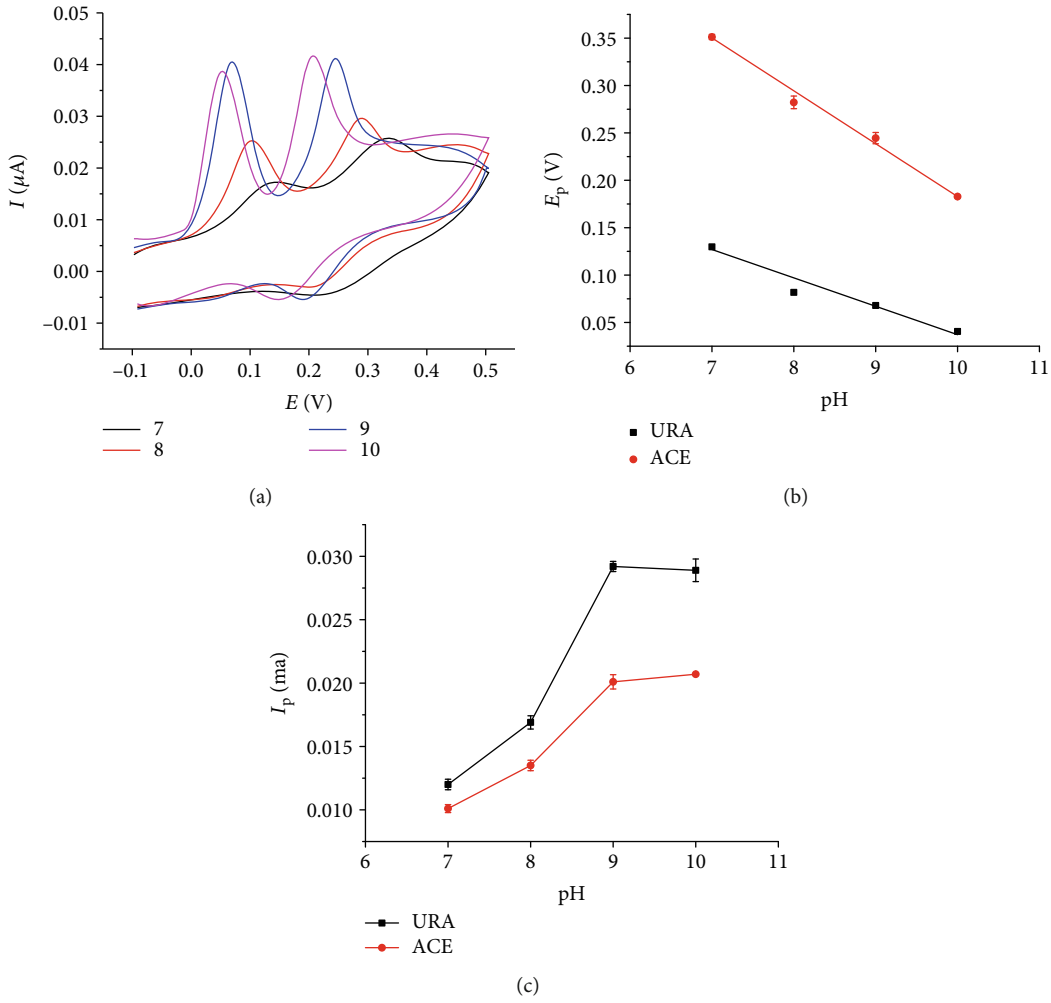

FIGURE 3: (a) CVs recording at ZIF-67/C_3N_4-GCE in 0.1 M BR-BS pH = 7 ÷ 10 containing equal concentrations of 0.5 mM URA, ACE, and 150 μM CTAB; (b) the plot of E_p vs. pH; (c) the plot of I_p vs. pH.

reaction is an adsorption-controlled or diffusion-controlled process (Figure 8(b)). If the linear plot of I_p vs. $\nu^{1/2}$ passes the origin, this process is controlled by diffusion; otherwise, it is an adsorption-controlled process [24]. The linear regression equations of I_p vs. $\nu^{1/2}$ are expressed as follows:

$$\begin{aligned} I_{p,URA} &= (-0.160 \pm 0.033) + (0.100 \pm 0.006) \times \nu^{1/2}, \\ &\quad r = 0.995, p < 0.001, \\ I_{p,ACE} &= (-0.023 \pm 0.019) + (0.091 \pm 0.011) \times \nu^{1/2}, \\ &\quad r = 0.979, p = 0.004. \end{aligned} \tag{3}$$

The linear relation of $I_{p,URA}$ and $I_{p,ACE}$ vs. $\nu^{1/2}$ is statistically significant ($r = 0.997 \div 0.999$, $p < 0.05$). The number in the parentheses represents the 95% confidence interval. The intercepts do not pass the origin because the 95% confidence interval for the intercept does not contain 0 (varying from −0.041 to −0.004 for ACE and from −0.072 to −0.006 for URA). This indicates that the electrode process of the URA and ACE electrooxidation is controlled by adsorption.

The linear regression equations of E_p vs. ln ν are as follows:

$$\begin{aligned} E_{p,URA} &= 0.112 + 0.026 \times \ln \nu, r = 0.984, \\ E_{p,ACE} &= 0.290 + 0.027 \times \ln \nu, r = 0.984. \end{aligned} \tag{4}$$

According to the Laviron theory [25], the relation of E_p vs. ln ν can be expressed as Equation (5) in an irreversible system:

$$E_p = E^0 - \frac{RT}{(1-\alpha)nF} \ln \frac{RTK_s}{(1-\alpha)nF} + \frac{RT}{(1-\alpha)nF} \ln \nu, \tag{5}$$

where α is the electron transfer coefficient, R is the universal constant (8.314 J/mol·K) at 298 K, and F is the Faraday constant (96,500 C·mol^{-1}). The slope of the line of E_p vs. ln ν provides the value of $(1-\alpha) \times n$ for ACE and URA being 0.95 and 0.99, respectively (Figure 8(c)). It is assumed that the value of α is 0.5. Then, the value of n is 1.9 for ACE and 1.98 for URA. Therefore, the equal number of electrons

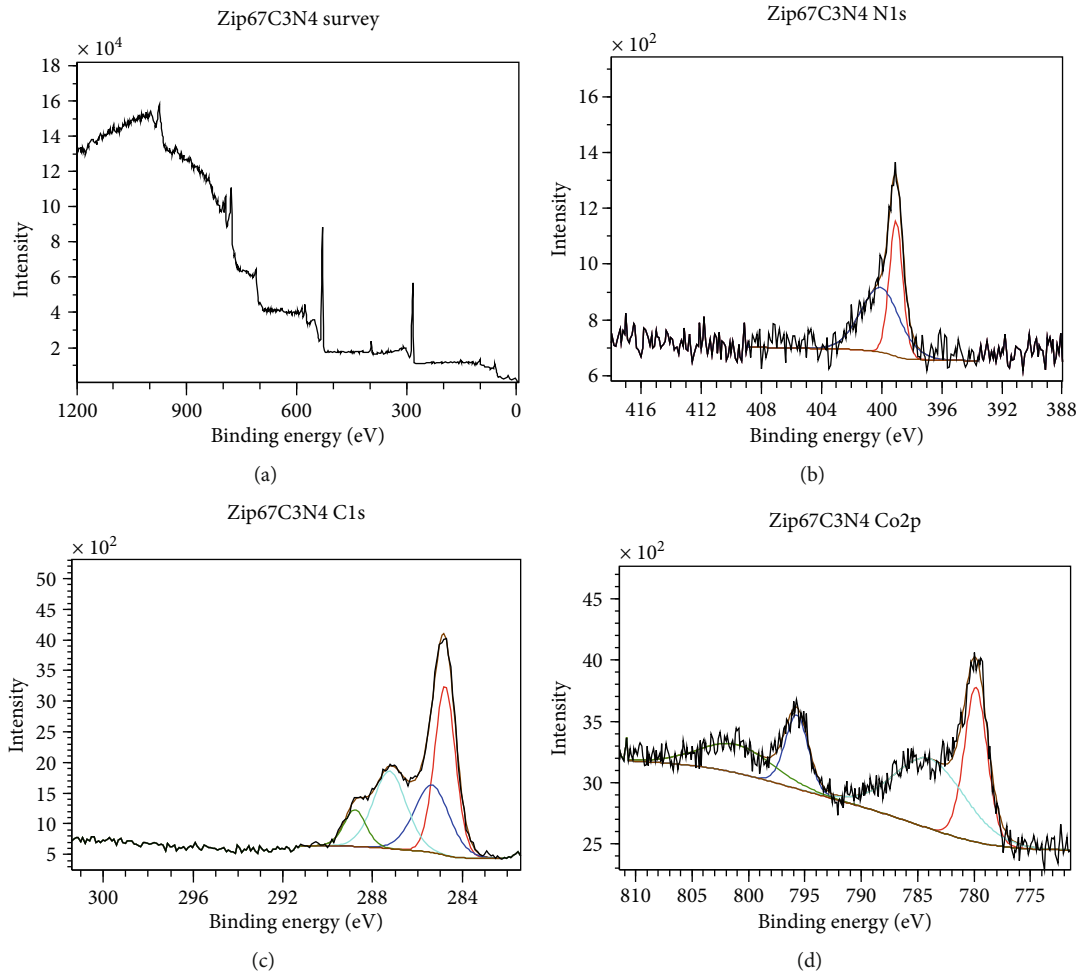

FIGURE 4: XPS spectra of ZIF-67/g-C_3N_4: (a) survey spectrum; (b) N1s XPS spectrum; (c) C1s XPS spectrum; (d) Co2p XPS spectrum.

transferred is 2 for ACE. This means that two electrons and two protons are involved in the ACE oxidation to form N-acetyl-p-quinone-imine [26] at the modified electrodes. In the case of URA, the ratio of the number of protons and transferred electrons is not equal to one and involves less protons than electrons, e.g., two electrons and one proton. Although the mechanism of URA at the modified electrode is nuclear, this could be explained as the inference due to uncertainties introduced by the close proximity of voltammetric peak to the background discharge probably due to oxidation undergoing deprotonation or the adsorption of oxidation products blocking the electrode at the studied pH.

The favorable signal-promoting effect indicates that CTAB enhances the discriminating peak current of ACE and URA. In this aspect, ZIF-67/g-C_3N_4 plays an important role in promoting the electron transfer rates of ACE and URA and brings out excellent electrocatalytic activity towards the *redox* reactions. Because ZIF-67 comprises imidazole rings of the sp^2-conjugated bond (π–π interaction), the π–π stacking interaction between the phenyl structures of URA and ACE and the three-dimensional imidazolate structure of ZIF-67/g-C_3N_4 favors the adsorption on the modified electrode surface. The coordination of the nitrogen atoms in the analytes with Co (II) ions attracts ACE and URA to the modified electrode surface. In addition, g-C_3N_4 facilitates electron mobility in the redox reaction. In addition, the CTAB as a discriminating agent is also contributed to the well-defined separation of electrochemical signals. Therefore, the combination of these effects promotes the transfer of electrons and results in enhancing voltammetric signals. The oxidation mechanism for ACE and URA at the modified electrodes is proposed in Figure 9.

3.3. Interference Study. Interferents commonly existent in biological samples include glucose, sucrose, oxalate, $CaCl_2$, $(NH_4)_2SO_4$, $NaNO_3$, $KHCO_3$, and K_2SO_4. Table 1 presents the tolerance limits of eight interferents. The tolerance limit, C_{tol}, is the concentration of the interferent that raises a relative error (RE) of 5% in the determination of 0.5 μM URA or 0.5 μM ACE. The findings show that the interference of inorganic salts is insignificant. However, some organic compounds, such as glucose, interfere but only at high concentrations. This indicates that the proposed method is likely to be free from common interferents in biological samples.

3.4. Long-Term Stability, Repeatability, and Linear Range. The long-term stability of the electrochemical response is of special interest for automatic monitoring of biological

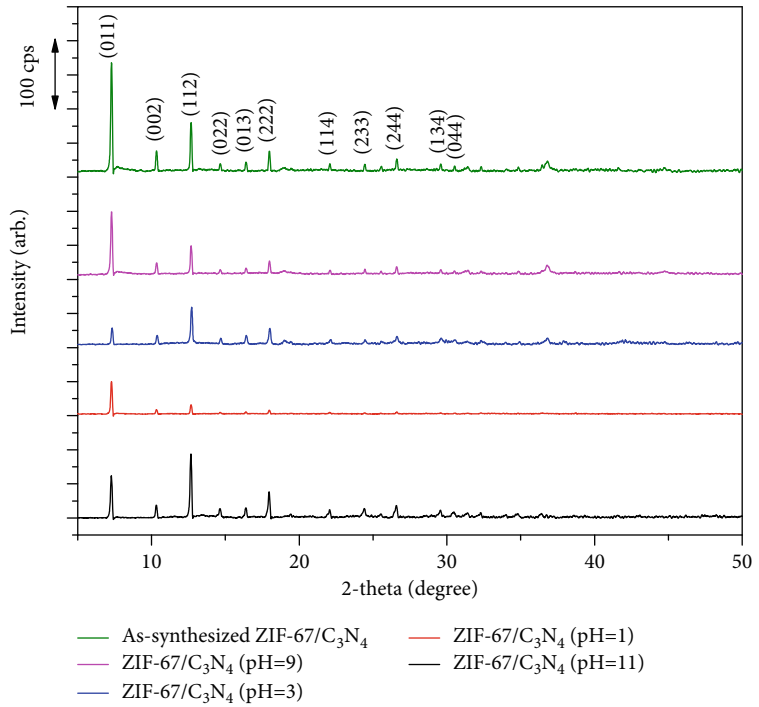

Figure 5: The stability of ZIF-67/g-C_3N_4 in water with different pH.

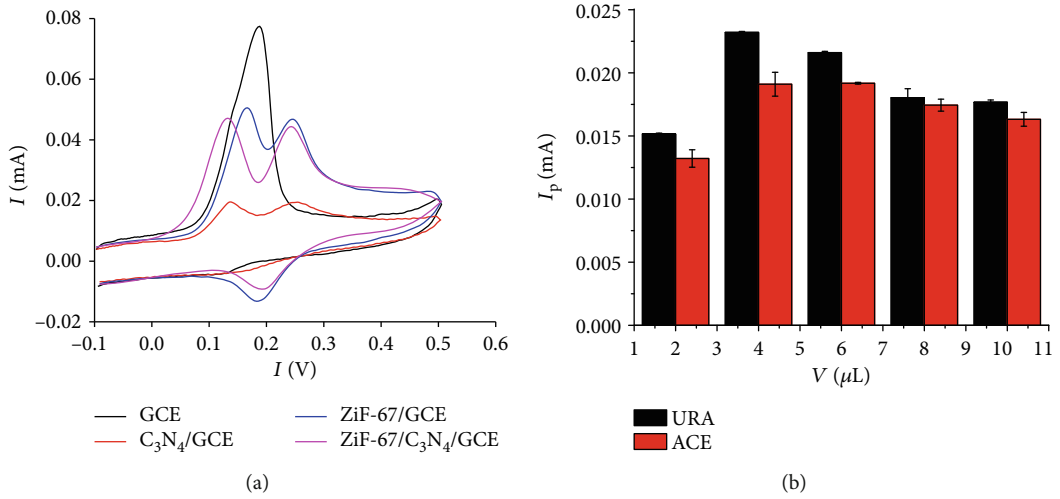

Figure 6: (a) CVs at different electrodes in 0.1 M BR-BS pH 9 containing equal concentrations of 0.5 mM URA and ACE; (b) effect of ZIF-67/g-C_3N_4 amount on anodic peak current.

analytes. Hence, the response of ZIF-67/g-C_3N_4 was performed for a ten-day period by immersing the electrode in a solution of spiked water with 0.1 M BR-BS pH 9 containing 150 μM CTAB, 0.2 μM URA, and 0.2 μM ACE (10 measurements were performed during the working-day period). The electrode was stored in the buffer solution between each analysis. The changes of average I_p versus time are presented in Figure 10. The RSDs (relative standard deviations) of I_p for URA and ACE were 7.72 and 7.02%, respectively, using the same electrode for all the measurements. These values were lower than $1/2RSD_H$ [27] indicating that the proposed DP-ASV method exhibits high stability.

The repeatability of the DP-ASV responses was evaluated by using a RSD for nine consecutive determinations of 5×10^{-7} M URA and 5×10^{-7} M ACE. The RSD of URA and ACE is 1.03 and 1.52, which is lower than $1/2RSD_{Hozit}$, indicating that the modified electrode shows good stability. The stability of the ZIF-67/g-C_3N_4-modified electrode was also tested by leaving the electrode in a desiccator under atmospheric conditions for 10 days. The DP-ASV peak currents

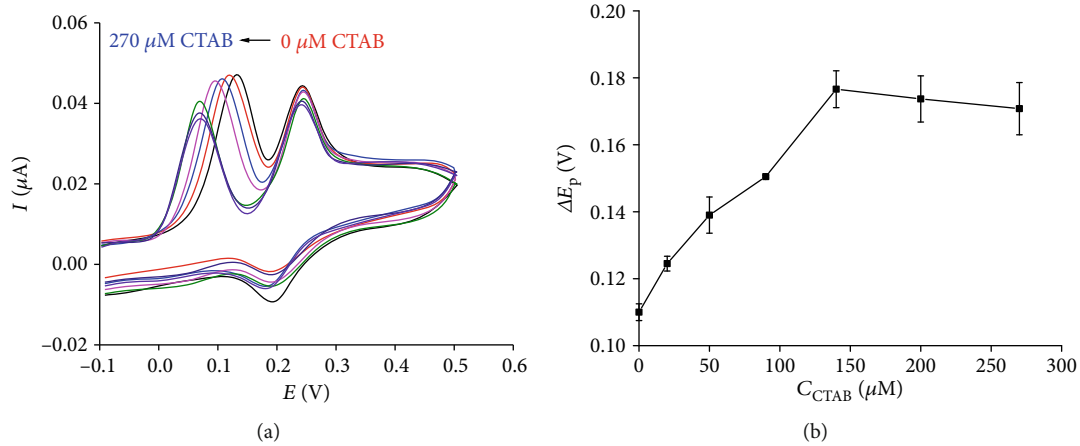

FIGURE 7: (a) CVs at ZIF-67/g-C_3N_4/GCE in 0.1 M BR-BS containing $C_{URA} = C_{ACE} = 0.5$ mM and various concentrations of CTAB; (b) peak-to-peak separation as a function of CTAB concentration.

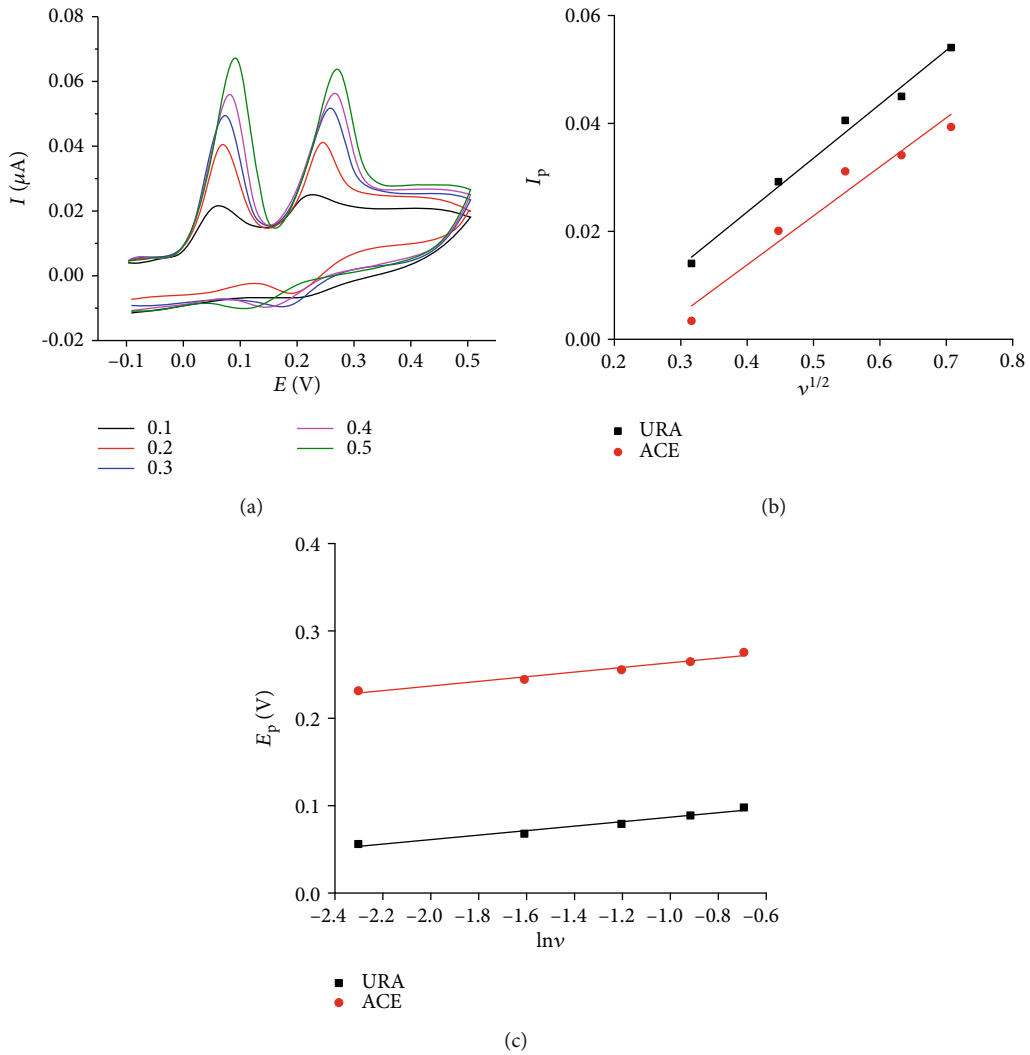

FIGURE 8: Scan rate dependence of peak potential and peak current (a); the linear plots of I_p vs. $\nu^{1/2}$ (b); E_p vs. ln ν (c); $C_{CTAB} = 150 \times 10^{-6}$ M and $C_{URA} = C_{ACE} = 0.5 \times 10^{-3}$ M in BR-BS buffer 0.1 M, pH 9.

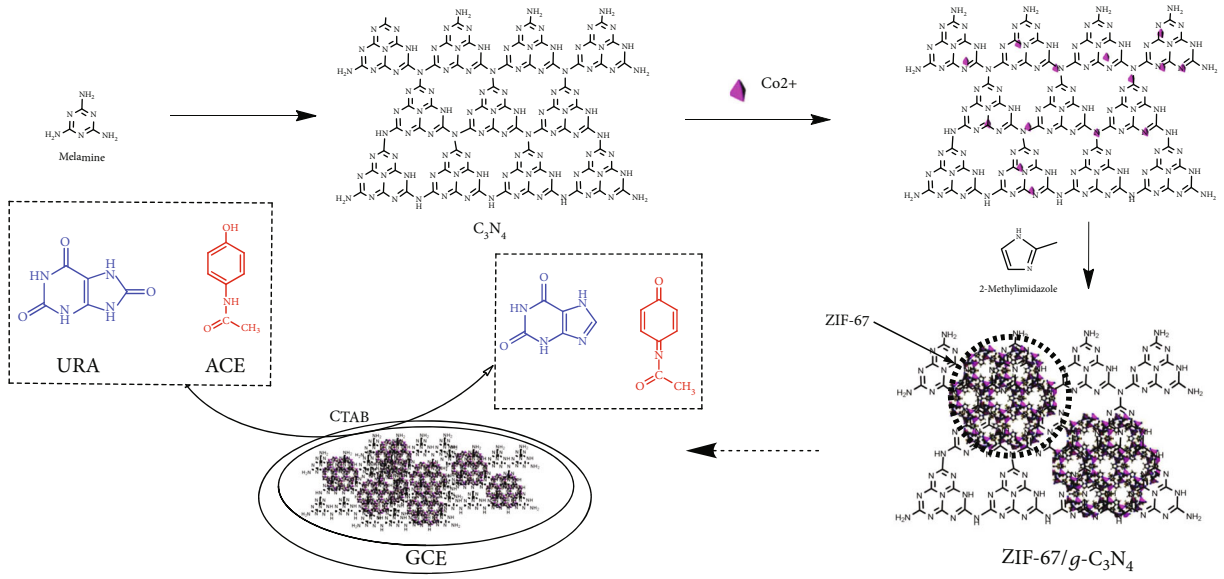

Figure 9: Proposed mechanism of URA and ACE oxidation at the ZIF-67/g-C_3N_4-modified electrode.

Table 1: Tolerance limits of interferents, C_{tot} ($5{\cdot}10^{-7}$ M URA or $5{\cdot}10^{-7}$ M URA in 0.1 M BR-BS pH 9 and 150 μM CTAB).

Interfering substances	C_{tot} (μM) URA (0.5 μM)	RE (%)	ACE (0.5 μM)	RE (%)
Glucose	75	−4.55	75	4.9
Sucrose	75	−4.30	75	4.99
Oxalate	75	−4.79	150	4.85
$NaNO_3$	150	−4.92	150	4.86
$CaCl_2$	100	2.49	100	−3.40
K_2SO_4	150	4.2	150	−3.1
$(NH_4)_2SO_4$	100	−3.26	100	4.38
$KHCO_3$	150	−4.32	150	3.19

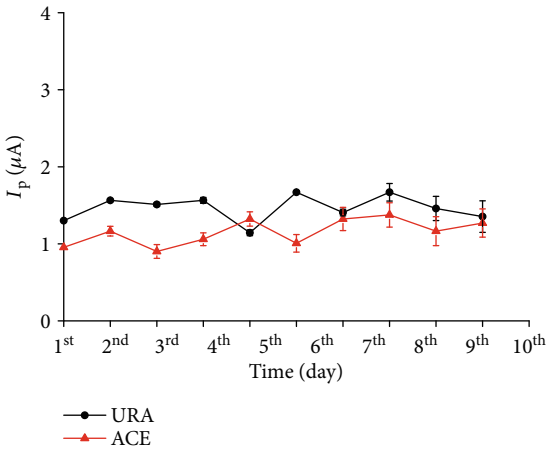

Figure 10: Long-term stability test for a ten-day period.

for 5×10^{-7} M URA and 5×10^{-7} M ACE decrease by less than 4.61 and 4.90%, respectively. The high stability of the ZIF-67/g-C_3N_4-modified electrode contributed to its high mechanical strength and high stability in water, making it a potential for practical applications.

The detection of each compound in the presence of the other was conducted. Figure 11(a) shows the DPV curves recorded when adding URA or ACE and keeping the other constant. The anodic peak current increases linearly ($I_{p,URA} = 0.09 + 5.69C_{URA}$, $r = 0.995$) with the concentration of URA from 0.02 to 0.65 μM in the presence of ACE with the limit detection (LOD) of 0.055 μM (Figure 11(b)). A similar behaviour is observed with the detection of ACE ($I_{p,ACE} = 0.15 + 5.63C_{ACE}$, $r = 0.997$) in the same concentration range with the detection limit of 0.056 μM (Figures 11(c) and 11(d)). Figure 12(a) represents the DP-DVS curves recorded for the simultaneous addition of URA and ACE in the concentration range between 0.02 and 0.65 μM. The plots of $I_{p,URA}$ and $I_{p,ACE}$ vs. the URA and ACE concentrations are shown in Figure 12(b). The linear regression equations are $I_{p,URA} = 0.06 + 5.81C_{URA}$, $r = 0.998$, and $I_{p,ACE} = 0.14 + 5.84C_{ACE}$, $r = 0.999$. The LODs of URA and ACE are 0.052 μM and 0.053 μM, respectively. The similarity in LOD of URA and ACE in the mixture and as an individual infers that no remarkable interference due to the oxidation of the compounds occurs.

The linear regression equations of the peak current vs. the analyte concentration are expressed as follows:

$$I_{p,URA} = (0.06 \pm 0.05) + (5.82 \pm 0.03) \times C_{URA}, r = 0.998,$$
$$I_{p,ACE} = (0.14 \pm 0.04) + (5.84 \pm 0.11) \times C_{ACE}, r = 0.999. \quad (6)$$

In the range from 0.02 to 0.65 μM for URA and ACE, the LODs of URA and ACE are 0.052 μM and 0.053 μM,

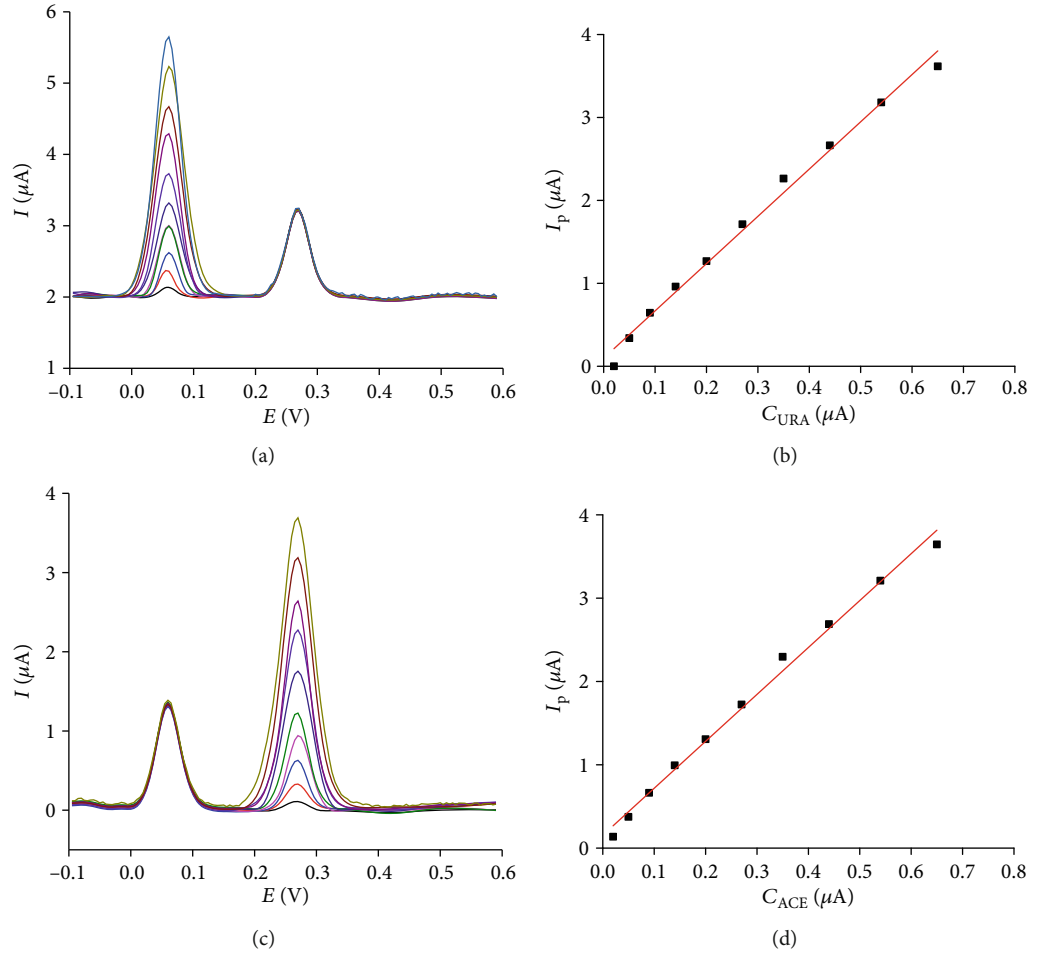

Figure 11: Differential pulse voltammetric responses at ZIF-67/g-C_3N_4-GCE in 0.1 M BR-BS pH 9 containing (a) 150 μM CTAB and 0.2 μM ACE; the URA concentration varying from 0.02 to 0.65 μM; (b) plot of anodic peak current as a function of URA concentration; (c) 150 μM CTAB, 0.2 μM URA; the ACE concentration varying from 0.02 to 0.65 μM; (d) plot of anodic peak current as a function of ACE concentration.

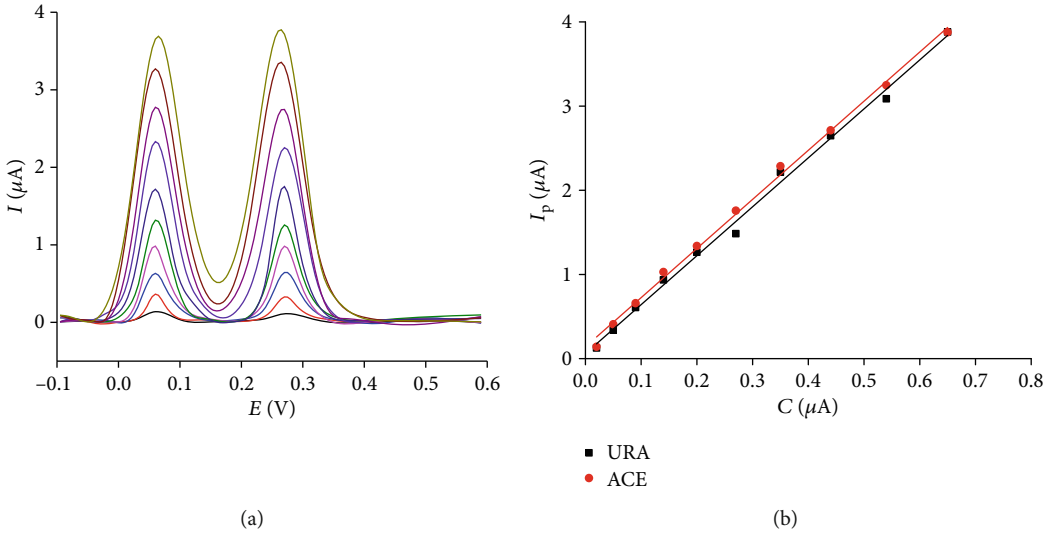

Figure 12: (a) DPVs recorded at ZIF-67/g-C_3N_4/GCE in 0.2 BR-BS pH 9 containing equal concentrations varying from 0.2 to 6.5 μM; (b) plot of anodic peak current as a function of analyte concentration.

Table 2: Comparison of some LOD and linear range of different modified electrodes for the determination of URA and ACE.

Electrode	Linear range (μM) (URA/ACE)	LOD (μM) URA	LOD (μM) ACE	Reference
Ionic liquid/CNT/chitosan-CGE	(2–450)/(1–400)	0.34	0.24	[28]
Thiol functional ferrocene derivative stabilized Au NP/carbon dot nanocomposite coupling with graphene-GCE	(0.6–9.2)/(0.5–46)	0.2	0.1	[29]
SWCNT/chitosan/ionic liquid nanocomposite-GCE	(3–320)/(2–200)	0.27	0.11	[30]
MCNT/chitosan composite-GCE	(10–400)/(2–250)	0.4	0.16	[31]
ZIF-67/g-C_3N_4-GCE	**(0.2–6.5)/(0.2–6.5)**	**0.052**	**0.053**	**The present study**

Notes: MCNT: multiwalled carbon nanotube; SWCNT: single-walled carbon nanotube; GCE: glassy carbon electrode.

Table 3: URA and ACE detection in urine samples obtained using the proposed method and HPLC.

Sample	Analytes	Added (μM)	Found[a] (μM)	Rev. (%)	HPLC (μM)
Urine #1	URA	0	22.69	99.4	—[a]
		10	32.63		32.77
	ACE	0	0	96.7	—
		10	9.67		9.81
Urine #2	URA	0	26.11	97.8	—
		10	35.89		35.92
	ACE	0	0	98.0	—
		10	9.80		9.85
Urine #3	URA	0	25.03	96.9	—
		10	34.72		34.81
	ACE	0	0	104.0	—
		10	10.4		9.80

[a]No analysis.

respectively. Table 2 shows the ability of the ZIF-67/g-C_3N_4 electrode for the URA and ACE determination compared with other reported electrodes. The present electrode has a much lower limit of detection for the determination of URA and ACE in comparison with most modified materials.

The ZIF-67/g-C_3N_4-modified electrode was utilized in the real sample analysis. Urine samples were collected from three healthy volunteers. The DPV results of the urine samples were obtained for URA and ACE in the BS solution, to which 10 μL of a URA and ACE stock solution was spiked to an electrochemical cell without any preliminary pretreatment. The amount of URA and ACE in the samples was determined with the calibration method using DPV and is presented in Table 3. The recovery of the proposed method varies in the acceptable range of 90–110%. The URA and ACE level in the samples was also tested using HPLC for comparison. The paired-sample t-test with $\alpha = 0.05$ shows that there is no significant difference between the DPV proposed method and HPLC ($t(5) = 0.215$; $p = 0.839$). This suggests that the proposed method enables to determine the URA and ACE level in the human urine with satisfactory results.

4. Conclusions

ZIF-67/g-C_3N_4 was synthesized using the ultrasonic-assisted approach. The obtained material exhibits a large specific surface area and high stability in pH ranging of 3 to 12. The ZIF-67/g-C_3N_4 electrode shows high stability and reproducibility in repetitive measurements. The proposed method provides satisfactory results for the detection of uric acid and acetaminophen in human urine. The method is time-competitive, easy to perform, highly stable, and sensitive with high detectability. All these features suggest that the proposed method is a potential candidate for practical applications.

Data Availability

The data used to support the findings of this study are available from the corresponding authors upon request.

Conflicts of Interest

The authors declare that they have no conflicts of interest.

Acknowledgments

This research is funded by Vietnam National Foundation for Science and Technology Development (NAFOSTED) under grant number 104.06-2018.15.

References

[1] J. M. Zen, J. J. Jou, and G. Ilangovan, "Selective voltammetric method for uric acid detection using pre-anodized Nafion-coated glassy carbon electrodes," *Analyst*, vol. 123, no. 6, pp. 1345–1350, 1998.

[2] R. M. De Carvalho, R. S. Freire, S. Rath, and L. T. Kubota, "Effects of EDTA on signal stability during electrochemical detection of acetaminophen," *Journal of Pharmaceutical and Biomedical Analysis*, vol. 34, no. 5, pp. 871–878, 2004.

[3] F. L. Martin and A. E. M. McLean, "Comparison of paracetamol-induced hepatotoxicity in the rat in vivo with progression of cell injury in vitro in rat liver slices," *Drug and Chemical Toxicology*, vol. 21, no. 4, pp. 477–494, 1998.

[4] N. H. Phong, T. T. T. Toan, M. X. Tinh, T. N. Tuyen, T. X. Mau, and D. Q. Khieu, "Simultaneous voltammetric determination of ascorbic acid, paracetamol, and caffeine using electrochemically reduced graphene-oxide-modified electrode,"

Journal of Nanomaterials, vol. 2018, Article ID 5348016, 15 pages, 2018.

[5] A. Kutluay and M. Aslanoglu, "An electrochemical sensor prepared by sonochemical one-pot synthesis of multi-walled carbon nanotube-supported cobalt nanoparticles for the simultaneous determination of paracetamol and dopamine," *Analytica Chimica Acta*, vol. 839, pp. 59–66, 2014.

[6] J. F. Rusling, "Controlling electrochemical catalysis with surfactant microstructures," *Accounts of Chemical Research*, vol. 24, no. 3, pp. 75–81, 1991.

[7] R. Vittal, H. Gomathi, and K. J. Kim, "Beneficial role of surfactants in electrochemistry and in the modification of electrodes," *Advances in Colloid and Interface Science*, vol. 119, no. 1, pp. 55–68, 2006.

[8] G. Alarcón-Angeles, S. Corona-Avendaño, M. Palomar-Pardavé, A. Rojas-Hernández, M. Romero-Romo, and M. T. Ramírez-Silva, "Selective electrochemical determination of dopamine in the presence of ascorbic acid using sodium dodecyl sulfate micelles as masking agent," *Electrochimica Acta*, vol. 53, no. 6, pp. 3013–3020, 2008.

[9] S. Q. Liu, W. H. Sun, and F. T. Hu, "Graphene nano sheet-fabricated electrochemical sensor for the determination of dopamine in the presence of ascorbic acid using cetyltrimethylammonium bromide as the discriminating agent," *Sensors and Actuators B: Chemical*, vol. 173, pp. 497–504, 2012.

[10] Y. Hou, J. Li, Z. Wen, S. Cui, C. Yuan, and J. Chen, "N-doped graphene/porous g-C_3N_4 nanosheets supported layered-MoS_2 hybrid as robust anode materials for lithium-ion batteries," *Nano Energy*, vol. 8, pp. 157–164, 2014.

[11] Z. Meng, Y. Xie, T. Cai, Z. Sun, K. Jiang, and W. Q. Han, "Graphene-like g-C_3N_4 nanosheets/sulfur as cathode for lithium-sulfur battery," *Electrochimica Acta*, vol. 210, pp. 829–836, 2016.

[12] L. Tan, J. Xu, X. Zhang, Z. Hang, Y. Jia, and S. Wang, "Synthesis of g-C_3N_4/CeO_2 nanocomposites with improved catalytic activity on the thermal decomposition of ammonium perchlorate," *Applied Surface Science*, vol. 356, pp. 447–453, 2015.

[13] G. Lu and J. T. Hupp, "Metal-organic frameworks as sensors: a ZIF-8 based Fabry-Pérot device as a selective sensor for chemical vapors and gases," *Journal of the American Chemical Society*, vol. 132, no. 23, pp. 7832-7833, 2010.

[14] L. Yang, L. Yu, M. Sun, and C. Gao, "Zeolitic imidazole framework-67 as an efficient heterogeneous catalyst for the synthesis of ethyl methyl carbonate," *Catalysis Communications*, vol. 54, pp. 86–90, 2014.

[15] P. M. Usov, C. McDonnell-Worth, F. Zhou, D. R. MacFarlane, and D. M. D'Alessandro, "The electrochemical transformation of the zeolitic imidazolate framework ZIF-67 in aqueous electrolytes," *Electrochimica Acta*, vol. 153, pp. 433–438, 2015.

[16] Y. Meng, L. Zhang, H. Jiu et al., "Construction of g-C_3N_4/ZIF-67 photocatalyst with enhanced photocatalytic CO_2 reduction activity," *Materials Science in Semiconductor Processing*, vol. 95, pp. 35–41, 2019.

[17] N. Tian, H. Huang, and Y. Zhang, "Mixed-calcination synthesis of $CdWO_4$/g-C_3N_4 heterojunction with enhanced visible-light-driven photocatalytic activity," *Applied Surface Science*, vol. 358, pp. 343–349, 2015.

[18] Y. He, J. Cai, T. Li et al., "Efficient degradation of RhB over $GdVO_4$/g-C_3N_4 composites under visible-light irradiation," *Chemical Engineering Journal*, vol. 215-216, pp. 721–730, 2013.

[19] M. Tahir, C. Cao, N. Mahmood et al., "Multifunctional g-C3N4Nanofibers: a template-free fabrication and enhanced optical, electrochemical, and photocatalyst properties," *ACS Applied Materials & Interfaces*, vol. 6, no. 2, pp. 1258–1265, 2014.

[20] Q. Xu, C. Jiang, B. Cheng, and J. Yu, "Enhanced visible-light photocatalytic H_2-generation activity of carbon/g-C_3N_4 nanocomposites prepared by two-step thermal treatment," *Dalton Transactions*, vol. 46, no. 32, pp. 10611–10619, 2017.

[21] Y. Zheng, Y. Jiao, Y. Zhu et al., "Hydrogen evolution by a metal-free electrocatalyst," *Nature Communications*, vol. 5, no. 1, pp. 1–8, 2014.

[22] X. Yan, L. Tian, M. He, and X. Chen, "Three-dimensional crystalline/amorphous Co/Co_3O_4 core/shell nanosheets as efficient electrocatalysts for the hydrogen evolution reaction," *Nano Letters*, vol. 15, no. 9, pp. 6015–6021, 2015.

[23] D. Barreca, C. Massignan, S. Daolio et al., "Composition and microstructure of cobalt oxide thin films obtained from a novel cobalt (II) precursor by chemical vapor deposition," *Chemistry of Materials*, vol. 13, no. 2, pp. 588–593, 2001.

[24] A. J. Bard and L. J. Falkner, *Electrochemical Methods: Fundamentals and Applications*, vol. 60, Wiley, New York, NY, USA, 2001.

[25] E. Laviron, "General expression of the linear potential sweep voltammogram in the case of diffusionless electrochemical systems," *Journal of Electroanalytical Chemistry*, vol. 101, no. 1, pp. 19–28, 1979.

[26] S. A. Kumar, C. F. Tang, and S. M. Chen, "Electroanalytical determination of acetaminophen using nano-TiO_2/polymer coated electrode in the presence of dopamine," *Talanta*, vol. 76, no. 5, pp. 997–1005, 2008.

[27] W. Horwitz and R. Albert, "The concept of uncertainty as applied to chemical measurements," *Analyst*, vol. 122, no. 6, pp. 615–617, 1997.

[28] S. Kianipour and A. Asghari, "Room temperature ionic liquid/multiwalled carbon nanotube/chitosan-modified glassy carbon electrode as a sensor for simultaneous determination of ascorbic acid, uric acid, acetaminophen, and mefenamic acid," *IEEE Sensors Journal*, vol. 13, no. 7, pp. 2690–2698, 2013.

[29] L. Yang, N. Huang, Q. Lu et al., "A quadruplet electrochemical platform for ultrasensitive and simultaneous detection of ascorbic acid, dopamine, uric acid and acetaminophen based on a ferrocene derivative functional Au NPs/carbon dots nanocomposite and graphene," *Analytica Chimica Acta*, vol. 903, pp. 69–80, 2016.

[30] M. Afrasiabi, S. Kianipour, A. Babaei, A. A. Nasimi, and M. Shabanian, "A new sensor based on glassy carbon electrode modified with nanocomposite for simultaneous determination of acetaminophen, ascorbic acid and uric acid," *Journal of Saudi Chemical Society*, vol. 20, pp. S480–S487, 2016.

[31] A. Babaei, D. J. Garrett, and A. J. Downard, "Selective simultaneous determination of paracetamol and uric acid using a glassy carbon electrode modified with multiwalled carbon nanotube/chitosan composite," *Electroanalysis*, vol. 23, no. 2, pp. 417–423, 2011.